Applicability of K_d for modelling dissolved ^{137}Cs concentrations in Fukushima river water: case study of the upstream Ota River

Kazuyuki Sakuma [*a,d], Hideki Tsuji [b], Seiji Hayashi [b], Hironori Funaki [a], Alex Malins [c], Kazuya Yoshimura [a], Hiroshi Kurikami [a, c], Akihiro Kitamura [a, c], Kazuki Iijima [a], Masaaki Hosomi [d]

[a] Sector of Fukushima Research and Development, Japan Atomic Energy Agency, 10-2, Fukasaku, Miharu-machi, Tamura-gun, Fukushima 963-7700, Japan,

[b] Fukushima Branch, National Institute of Environmental Studies, 10-2, Fukasaku, Miharu-machi, Tamura-gun, Fukushima 963-7700, Japan,

[c] Center for Computational Science & e-Systems, Japan Atomic Energy Agency, University of Tokyo Kashiwanoha Campus Satellite, 178-4-4 Wakashiba, Kashiwa-shi, Chiba 277-0871, Japan,

[d] Department of Chemical Engineering, Tokyo University of Agriculture and Technology, 2-24-16 Naka, Koganei, Tokyo 184-8588, Japan,

Correspondence to K. Sakuma: sakuma.kazuyuki@jaea.go.jp

Highlights

- Study on validity of using the K_d absorption/desorption model for simulating dissolved ^{137}Cs levels in a Fukushima river.
- Agreement generally good between simulations and observations for water, sediment and particulate ^{137}Cs discharge.
- Tuning of K_d values for large particles was necessary for simulations to reproduce typical base flow dissolved ^{137}Cs concentrations.
- Simulations underestimated the seasonal variability of dissolved ^{137}Cs concentrations and peaks during heavy rainfall.

Abstract

A study is presented on the applicability of the distribution coefficient (K_d) absorption/desorption model to simulate dissolved ^{137}Cs concentrations in Fukushima river water. The upstream Ota River basin was simulated using GEneral-purpose Terrestrial Fluid-flow Simulator (GETFLOWS) for the period 1 January 2014 to 31 December 2015. Good agreement was obtained between the simulations and observations on water and suspended sediment fluxes, and on particulate bound ^{137}Cs concentrations under both base and high flow conditions. By contrast the measured concentrations of dissolved ^{137}Cs in the river water were much harder to reproduce with the simulations. By tuning the K_d values for large particles, it was possible to reproduce the mean dissolved ^{137}Cs concentrations during base flow periods (observation: 0.32 Bq/L, simulation: 0.36 Bq/L). However neither the seasonal variability in the base flow dissolved ^{137}Cs concentrations (0.14-0.53 Bq/L), nor the peaks in concentration that occurred during storms (0.18-0.88 Bq/L, mean: 0.55 Bq/L), could be reproduced with realistic simulation parameters. These discrepancies may be explained by microbial action and leaching from organic matter in forest litter providing an additional input of dissolved ^{137}Cs to rivers, particularly over summer, and limitations of the K_d absorption/desorption model. It is recommended that future studies investigate these issues in order to improve simulations of dissolved ^{137}Cs concentrations in Fukushima rivers.

1. Introduction

Cesium-137 is discharged from contaminated watersheds in Fukushima Prefecture in either the dissolved or particulate form. Field monitoring surveys have concluded that from ~2013 onwards the majority of ^{137}Cs export from Fukushima's river basins occurs via particulate discharge (Nagao et al., 2013, 2015; Ueda et al., 2013; Yamashiki et al., 2014; Yoshikawa et al., 2014; Sakaguchi et al., 2015; Iwagami et al., 2016). Particulate discharge occurs readily in typhoon storms, as saturated ground leads to surface run-off, sediment erosion and input to rivers (Nagao et al., 2013; Ueda et al., 2013; Evrard et al., 2015).

Dissolved ^{137}Cs transport cannot be overlooked however (Eyrolle-Boyer et al., 2016). In the initial year following the fallout, the dissolved fraction accounted for 8-55% of the total discharge from various basins (Nagao et al., 2013; Ueda et al., 2013; Yamashiki et al., 2014). The relative contribution of the dissolved component decreased in the years that followed to 1-30% of the total discharge (including typhoon periods). However this can still represent a large quantity of ^{137}Cs discharge in absolute terms (Evrard et al., 2015; Sakaguchi et al., 2015; Iwagami et al., 2016; Tsuji et al., 2016), especially for the highly contaminated basins surrounding the Fukushima Dai-ichi Nuclear Power Plant (FDNPP) where ^{137}Cs contamination levels exceed 1 MBq/m^2 (Saito et al., 2015; Sakuma et al., 2017).

Various field monitoring studies have concluded that dissolved ^{137}Cs discharge is most significant during the extended base flow periods between typhoons. Under base flow conditions the dissolved fraction represents between 16 and 91% of the total discharge through rivers (Ochiai et al., 2015, Eyrolle-Boyer et al., 2016; Tsuji et al. 2016). As river water is extracted for agricultural, fish farming and industrial purposes across Fukushima Prefecture, a clear understanding of the factors affecting dissolved ^{137}Cs concentrations is needed. In particular Yoshikawa et al. (2014) found that the uptake of ^{137}Cs by rice plants was associated with the concentration of dissolved ^{137}Cs in the water used to irrigate the plants, and Uematsu

et al. (2017) demonstrated in experiment that rice takes up ^{137}Cs from contaminated irrigation water, supporting the conclusion of Nakanishi et al. (2013).

Dissolved ^{137}Cs concentrations in Fukushima rivers are highly correlated with the fallout inventories of the catchments (Tsuji et al., 2014a; Ochiai et al., 2015; Yoshimura et al., 2015b; Eyrolle-Boyer et al., 2016). Yoshimura et al. (2015b) reported that the concentration of dissolved ^{137}Cs in river water was correlated with the ^{137}Cs concentration in suspended solids. This result implies that it is reasonable to model ^{137}Cs absorption and desorption between the dissolved and bound states with distribution coefficients (K_d) (Zheleznyak et al., 1992; Kurikami et al., 2014, 2016; Mori et al., 2015; Sakuma et al., 2017, 2018). Various simulation studies of dissolved ^{137}Cs concentrations in river basins contaminated by Chernobyl accident fallout were undertaken using K_d (Zheleznyak et al. 1992; Onishi et al, 2007). Another approach is to use empirical models for ^{137}Cs absorption/desorption (Nylén and Grip, 1997; Monte et al., 2014).

On the other hand, Ochiai et al. (2015) reported a weak correlation between dissolved and particulate ^{137}Cs concentrations in the water of seven Fukushima rivers under base flow conditions. Shinomiya et al. (2014), Yoshikawa et al. (2014), and Tsuji et al. (2016) reported that dissolved ^{137}Cs concentrations increased during typhoon storms compared to base flow levels. Furthermore Tsuji et al. (2016) reported a seasonal variability of dissolved ^{137}Cs concentrations under base flow conditions. To date no studies have been published on applicability of K_d for simulating dissolved ^{137}Cs concentrations in rivers in Fukushima Prefecture (Mori et al., 2015).

The purpose of this study was to see whether simulations employing the K_d model could reproduce the variations in dissolved ^{137}Cs concentrations in occur in a Fukushima river. The upstream Ota River catchment was chosen for study due to the availability of various field data by Tsuji et al. (2016). The herein described simulations were calibrated against measurements

by Tsuji et al. (2016), as well more recent, previously unpublished, monitoring results.

2. Method

2.1 Study area

The upstream Ota catchment covers 21 km^2 and lies 24.4 km northwest of the FDNPP site, as shown in Fig. 1 (Tsuji et al., 2016). The mean ^{137}Cs inventory of the study area was ~1.9 MBq/m^2 in July 2011, based on the third airborne monitoring survey (Ministry of Education, Culture, Sports, Science and Technology Japan, 2011). Forests, mainly cedar and oak, cover 99.2% of the catchment area (Ministry of the Environment, 2016). The surface soil is predominantly brown forest soil (Ministry of Land, Infrastructure and Tourism, 2016). The bedrock is mostly granite and diorite (National Institute of Advanced Science and Technology, 2016). The catchment lies within the difficult to return to evacuation zone (Ministry of Economy, Trade and Industry, 2017), and decontamination work has not taken place. Factors pertaining to decontamination and the effects of a resident population therefore do not need to be considered when interpreting dissolved ^{137}Cs concentrations in the river water (Evrard et al., 2014).

The outflow from the catchment drains to the Yokokawa dam reservoir, and then on towards agricultural and urban land in the Minamisoma area. Water is extracted from the Ota River for irrigation, yamame salmon farming and industrial use in the downstream, repopulated areas.

2.2 Simulation model and parameters

The General-purpose Terrestrial fluid-FLOW Simulator (GETFLOWS) was used to model the catchment. This code has previously been used to simulate the Odaka, Ukedo, Maeda, Kuma and Tomioka River and Hokkawa Dam basins in Fukushima Prefecture (Mori et al., 2015; Kitamura et al., 2016; Sakuma et al., 2017, 2018) The simulations in those studies were

validated using measurements of water, suspended sediment and sediment-sorbed ^{137}Cs discharge from the catchments. However there have been no studies to date examining GETFLOWS results for dissolved ^{137}Cs discharge, which are based on the K_d model.

A three dimensional hydraulic geological model was developed for the upstream Ota River catchment (Fig. 2) by combining surface topography data from the Geospatial Information Authority of Japan (2012) and subsurface geology data from the Geological Survey of Japan (2012). The land surface was segregated into 13,104 cells with sides averaging 40 m width and breadth. Sand control dams in the upstream of the catchment (Fig. 1) could not be modeled as these features are smaller than the created grid cells. There was one air layer, one surface layer and 20 sub-surface layers in the model (total 288,288 grid-blocks).

Mori et al. (2015) outlines the various components of GETFLOWS and lists the equations of water, sediment and ^{137}Cs flows that the code solves. In summary, the code calculates surface water flows, sub-surface air and water flows, and sediment transport via soil erosion, suspension within surface water flows and re-deposition. Cesium-137 transport was calculated in both the particulate and dissolved forms. The various input parameters used in the simulations herein are listed in Tables S1 to S6. These parameters are similar to the parameters used in Sakuma et al. (2017, 2018). The exceptions are the parameters highlighted with bold font in Tables S4 to S6. These parameters were tuned especially for this study such that the simulations matched both the peak water discharge rates and suspended sediment fluxes in storms over the study period.

The conservation law for dissolved ^{137}Cs transport is

$$-\nabla\cdot\left(M_w R_{cw}\right)+\nabla\cdot D_{cw}\nabla\left(\rho_w R_{cw}\right)-\rho_w q_w R_{cw}-\lambda\rho_w\phi S_w R_{cw}$$
$$+\rho_w R_{ss,i} m_i^{adsorp}+\rho_{ss,i}(1-\phi)m_i^{adsorp}=\frac{\partial}{\partial t}\left(\rho_w\phi S_w R_{cw}\right) \quad (1)$$

The rate of change of the dissolved ^{137}Cs concentration in each grid-block, right hand side of the equation, is the sum of various factors. The first two terms on the left hand side of the

equation represent advective and dispersive flows, respectively. M_w is the water mass flux (kg/m^2/s), R_{cw} is the mass fraction of dissolved ^{137}Cs in the water (kg/kg), D_{cw} is the coefficient of hydrodynamic dispersion (m^2/s), and is ρ_w the density of water (kg/m^3). The following two terms on the left hand side of Eq. (1) model sources and sinks, and radioactive decay. q_w is the volumetric flux of water sinks and sources (m^3/m^3/s), λ is the decay constant of ^{137}Cs (1/s), ϕ is the effective porosity (m^3/m^3), and S_w is the saturation factor (m^3/m^3).

The final two terms on the left hand side of Eq. (1) represent the transfer of ^{137}Cs between the dissolved and particulate fractions. $R_{ss,i}$ is the mass fraction of suspended sediment particle grade i within the water (kg/kg), m_i^{adsorp} is a rate of absorption/desorption of dissolved to/from particulate-bound ^{137}Cs, and $\rho_{ss,i}$ is the density of sediment grade i (kg/m^3). The first term applies to the surface layer cells, where adsorption/desorption can occur to suspended sediments within surface water. The second term applies to the sub-surface layers where adsorption/desorption can occur to soil particles. The rate of absorption and desorption is given by

$$m_{ss,i}^{adsorp} = a_i^{1,2}\left(K_{d,i}R_{cw} - R_{cs,i}\right) \qquad (2)$$

where $a_i^{1,2}$ is the rate constant (1/s), $K_{d,i}$ is the ^{137}Cs distribution coefficient between the dissolved and bound states (kg/kg), and $R_{cs,i}$ is the mass fraction of ^{137}Cs bound to the particulates (kg/kg).

Data from the eighth airborne monitoring survey conducted between 2-19 November 2013 were used to initialize the ^{137}Cs inventory in each cell of the model. The data for ambient dose equivalent rates at 1 m above the ground surface ($\dot{H}^*(10)$ – μSv/h) were converted to ^{137}Cs inventories per unit land area (Bq/m^2) as follows. An exponential depth distribution for ^{137}Cs in soil was assumed with relaxation mass depth β = 2.0 g/cm^2. This value, applicable on 14 November 2013, was interpolated from measurements of β from soil scraper plate sampling across Fukushima Prefecture (Malins et al., 2016). Dose rates were then converted to ^{137}Cs

165 inventories using conversion coefficients from Saito and Petoussi-Henss (2014), accounting for
166 the contributions from natural background radiation (0.05 μSv/h) and ^{134}Cs to the measured
167 dose rates.

168 GETFLOWS is limited to modeling ^{137}Cs with fixed activity concentrations in the surface
169 and sub-surface layers. Constant ^{137}Cs radioactivity concentrations down to a depth of 2 cm
170 below the surface, and zero radioactivity further below, were assumed as the initial values for
171 the simulations. The choice of a 2 cm thick topsoil layer was made for computational reasons,
172 i.e. few soil layers so that the simulations converged on reasonable timescales. Although
173 simulating with finer resolution topsoil layers is desirable, assigning all the ^{137}Cs to the top
174 2 cm of soil is reasonable as measurements show the majority of ^{137}Cs in forest soils is located
175 within the surface layer (Ministry of Agriculture, Forestry and Fisheries, 2015; Yoschenko et
176 al., 2017; Takada et al., 2017). The initial ^{137}Cs activity in the cells covered by more than 2 cm
177 of surface water was zero as the initial condition. The activity density per land area (Bq/m^2)
178 was assigned for each cell based on the nearest airborne monitoring survey datum.

179 Our model did not include forest-specific compartments for ^{137}Cs storage and transfer,
180 such as the forest canopy, litter layer and tree bodies. Therefore the inventories of coniferous
181 and broad leaf forests were reduced by factors of 0.73 and 0.78, respectively, to account for the
182 inventory that was not available for mobilization in the simulations (Ministry of Agriculture,
183 Forestry and Fisheries, 2015). The implications of the inventory contained within the forest
184 biomass and litter layer being unavailable for mobilization in the simulations are discussed
185 further in section 4.

186 The partitioning of the ^{137}Cs inventory between the particulate and aqueous phases was
187 modeled with the distribution coefficients $K_{d,i}$ in Table 1, where i denotes different particle
188 grades. GETFLOWS models six particle grades with representative diameters of 0.001, 0.01,
189 0.1, 0.3, 1 and 5 mm. The distribution coefficients were set at 0 L/kg for the 1 and 5 mm

diameter grades due to the low affinity for large particles to bind ^{137}Cs. Equilibrium partitioning between the dissolved and particulate fractions was assumed at the start of the simulation.

In the first simulation (case 1) the distribution coefficients for the 0.001-0.3 mm grades was set at 2.0 x 10^5 L/kg. This was based on the partitioning between dissolved ^{137}Cs and bound ^{137}Cs in suspended solids measured from river water samples taken at the catchment outflow during three typhoons on 6 October 2014, 14 October 2014 and 16 July 2015 (2.0 x 10^5 ± 7.7 x 10^4 L/kg, n=24) by Tsuji et al. (2016). The case 1 simulation gave dissolved ^{137}Cs concentrations at the outflow which tended to be lower than the observed values in both base flow and storm periods. Therefore a second simulation (case 2) was performed where the distribution coefficient for the 0.1 and 0.3 mm grades was lowered to 5.0 x 10^4 L/kg, in order that the simulations matched the dissolved ^{137}Cs concentrations measured by Tsuji et al. (2016) in fall 2014. The second K_d dataset is more realistic for modeling ^{137}Cs absorption to the particulates, as absorption occurs more readily to the finer grades than the coarser grades (Livens and Baxter, 1988; He and Walling, 1996).

The water and sediment flows over the catchment were equilibrated prior to commencing the production simulations (cases 1 and 2) as follows. The annual average precipitation (3.67 mm/day) and evapotranspiration (1.34 mm/day) were calculated using weather data from the Haramachi (1976-2015) and Namie (1981-2010) weather stations (Japan Meteorological Agency, 2015) using the Hamon method (Hamon, 1961). These values were applied until the simulation flows attained a steady state.

The production simulations covered the period 1 January 2014 to 31 December 2015. Hourly rainfall data measured near the center of the catchment (further information in Tsuji et al., 2016) were inputs over the course of the simulations. Air temperature, sunshine duration, and average wind velocity data from the Haramachi weather station (Japan Meteorological Agency, 2014, 2015) and relative humidity data from the Fukushima weather station (Japan

Meteorological Agency, 2014, 2015) were used to calculate evapo-transpiration, snowfall and snowmelt according to the energy balance equation for the surface cells in the model. The air temperature lapse rate was 0.0057°C m^{-1}. Precipitation was either assigned as rain or snow depending on the temperature of the surface layer cell. Rainfall occurred when surface cell temperatures were greater than 1.5°C, and snowfall otherwise. Melting of accumulated snow in surface cells occurred when cell temperatures rose above 1.5°C.

2.3 Field sampling and monitoring methods

The monitoring results used to calibrate the simulations include data from Tsuji et al. (2016) covering January 2014 to July 2015, and previously unpublished results covering August to December 2015 (Table S7). To measure dissolved and particulate ^{137}Cs concentrations, 20-40 L samples of river water were extracted from the center of the outflow river of the catchment using a bucket (location shown in Fig. 1). Samples were taken at 2-4 weeks intervals between 22 January 2014 and 11 December 2015 (n=33) in base flow periods. When Typhoons Phanfone and Vongfong hit the catchment on 6 October 2014 and 14 October 2014, respectively, river water samples were collected from a nearby bridge at 1 h intervals (n=9). When Typhoon Nangka hit the catchment on 16 July 2015, 3 L river water samples were collected at 5-40 min intervals (n=15) using an auto water sampler (ISCO 6712, Teledyne Isco, Lincoln, NE, USA).

The water flow rate at the catchment outflow was calculated by the Yokokawa Dam Controlling Office by converting the water depth measured against a gauge using the equation

$$Q = 38.8h^{1.81} \qquad (3)$$

Here Q is the water flow rate (m^3/s) and h is the water depth (cm). The depth measurements were taken at 1 h intervals over the study period (or at 10 min intervals during high flow periods).

A turbidity meter (TC-500, Optex Co. Ltd., Shiga, Japan) was used to collect turbidity data (FTU) at 5-10 min intervals between 29 May 2014 and 10 September 2015. A linear equation

converting turbidity and suspended solids concentrations was established by least squares regression of *n*=48 river water samples.

2.4 Measurement of ^{137}Cs

The particulate fraction was separated first from the river water samples using nonwoven fabric cartridge filters with a 1 μm pore size (RP13-011; Japan Vilene Co. Ltd., Tokyo, Japan) (Tsuji et al., 2014b). During storm periods, large debris such as leaves and branches were removed from the samples before pumping into the cartridge filter device. The dissolved ^{137}Cs was separated from the remaining solution using cartridge filters impregnated with potassium zinc ferrocyanide (Yasutaka et al., 2015).

Measurements of ^{137}Cs radioactivity on the cartridge filters were performed using Canberra GC2518 (Canberra Japan, Tokyo, Japan) and Seiko SEG-EMS GEM 35-70 (Seiko EG&G Co. Ltd., Tokyo, Japan) coaxial high purity germanium detectors. The instruments were calibrated using Japan Radioisotope Association MX033U8PP (Tokyo, Japan) and Eckert & Ziegler EG-ML (Valencia, CA, USA) standard radioisotope sources. The ^{137}Cs radioactivity measurements for each filter were decay corrected to the sampling date. After gamma spectroscopy analysis, the cartridge filters containing suspended solids were dried in an oven at 105°C for 24-48 h to calculate the dry weight of the suspended solids.

3. Results

3.1 River water, suspended sediment fluxes, and ^{137}Cs discharge at the catchment outlet

The simulation results for the hourly mean water discharge rate at the catchment outlet were in good agreement with the field monitoring results for the majority of the two year study period (Fig. 3). The Nash-Sutcliffe efficiency of the two datasets is 0.75. The discharge ratio for the catchment for 2014, defined as the ratio of the cumulative discharge volume and the catchment area, was 1225 mm from the simulations and 1050 mm from the observations. The

corresponding results for 2015 were 1345 mm and 1148 mm, respectively. The main discrepancies occur in the early months of 2014 and 2015, i.e. during the snowfall and snowmelt seasons. The simulations tended to underestimate the water discharge rate for these periods, either due to erroneously modeling rainfall as snowfall, or underestimating the rate of snowmelt.

The simulations reproduced the observed hourly mean suspended sediment fluxes with reasonable accuracy, see Fig. 4 (measurements cover 29 May 2014 to 10 September 2015). The simulation result for total amount of sediment discharge over the study period was 2.9×10^9 g, which compares well with the monitoring result of 2.0×10^9 g. The underestimation of the peak that occurred in February 2015 correlates with the underestimation of the water discharge rate over the same period (cf. Fig. 3), and can be attributed to incorrect simulation of the precipitation type.

The water and suspended sediment fluxes over Typhoons Phanfone (6 October 2014), Vongfong (14 October 2014), and Nangka (16 July 2015) are shown separately in Fig. 5. The simulations in general gave good results for the peak fluxes over the storms except for the suspended sediment fluxes over Typhoon Nangka. The simulations tended to overestimate the suspended sediment fluxes as the storms subsided. A similar discrepancy was reported by Kitamura et al. (2016), who suggested a problem with the transport capacity model for suspended sediments. Another underlying cause may be the sand control dams upstream of the measurement point (Fig. 1) acting to reduce sediment discharge at low water flow rates. These dams were not included in the GETFLOWS model of the study area.

3.2 Dissolved and particulate ^{137}Cs concentrations in the catchment outflow

Under base flow conditions in the spring, summer and early autumn periods, the simulation with the first K_d parameter set (case 1, orange line, Fig. 6) underestimated the observed concentrations (0.14-0.53 Bq/L, mean: 0.32 Bq/L) of dissolved ^{137}Cs in the catchment outflow (red markers, Fig. 6). The case 1 simulation results were however reasonably consistent with

289 the observed values over the winter months. Conversely the case 2 simulation results with the
290 adjusted K_d parameter set (blue line, Fig. 6) matched the observations more closely during the
291 summer and fall seasons, in accordance with the desired tuning outcome (mean: 0.36 Bq/L).
292 However the case 2 simulation results were generally larger than the measurement results for
293 the winter periods. Figure S1 shows a scatter plot of measured and simulated dissolved ^{137}Cs
294 concentrations at the catchment outflow under base flow conditions (n=33). For case 1, 79% of
295 the results are within a factor of 2 of the measurements. The corresponding result for case 2
296 91%. The Pearson correlation coefficient is slightly higher for case 2 than for case 1 (Table S8).
297 Neither of the simulation cases succeeded in reproducing the seasonal variability in dissolved
298 ^{137}Cs concentrations observed at the outlet (red markers, Fig. 6). Moreover, the measurements
299 show a decreasing trend in dissolved ^{137}Cs concentrations from 2014 to 2015, which is not
300 evident in the simulation results (either case 1 or 2).

301 When the results for Typhoons Phanfone, Vongfong, and Nangka are examined
302 specifically (Fig. 7), it is clear that the simulations failed to reproduce the commensurate peaks
303 in dissolved ^{137}Cs concentrations (0.18-0.88 Bq/L, mean: 0.55 Bq/L) at the catchment outlet.
304 This result is in contrast to the concentrations of particulate bound ^{137}Cs, where the simulations
305 show peaks in the concentrations during storm periods, as per the measurement results (Fig. 7).
306 Possible causes of the discrepancies are examined in the Discussion section 4.

307 **3.3 Results on ^{137}Cs redistribution over the catchment**

308 The simulation results for the total dissolved ^{137}Cs discharge form the catchment outlet
309 between 29 May 2014 and 29 May 2015 were in good agreement with the measurements by
310 Tsuji et al. (2016), see Table 2. The case 2 simulation result (7.9 x 10^9 Bq) was in better
311 agreement with the measurement result (8.7 x 10^9 Bq) than the case 1 simulation (4.0 x 10^9 Bq).
312 This is a consequence of tuning process for the K_d values for the case 2 simulation. The K_d
313 values were adjusted such that the results from case 2 matched the observed dissolved ^{137}Cs

concentrations for the spring, summer and early autumn periods. On the other hand, the simulation results for the total sediment-sorbed ^{137}Cs discharge were 2 to 3.5 times larger than the observation result (Table 2). This is a consequence of the overestimation of suspended sediment fluxes (Fig. 5) and particulate ^{137}Cs fluxes (Fig. 7) as floods subside.

Yoshimura et al. (2015a) reported that 0.07% of the ^{137}Cs inventory in a forest Universal Soil Loss Equation (USLE) run-off plot was discharged bound to particulates between 17 July 2011 and 18 November 2012. Niizato et al. (2016) reported results between 0.04% and 0.12% for various forest ULSE plots over periods ranging between 143 days and 234 days in 2013 and 2014. The simulation results for the particulate ^{137}Cs discharge ratio from 29 May 2014 to 29 May 2015 for the entire upstream Ota catchment were 0.12% (case 1) and 0.18% (case 2).

Figure S2 shows the net change in ^{137}Cs inventory from 1 January 2014 to 31 December 2015 across the catchment. Cesium-137 tends to accumulate along river beds and in riparian zones within the catchment, and conversely be eroded from the forest areas. These results are consistent with GETFLOWS simulations for other catchments (Sakuma et al., 2017, 2018).

4. Discussion

4.1 Modeling dissolved ^{137}Cs concentrations with K_d

The effect of the K_d absorption/desorption model can be considered separately for the subsurface cells (pore water) and the surface cells (surface flows and rivers). The dissolved ^{137}Cs concentrations in pore water remain essentially constant over time for each subsurface cell in the model, because the rate of absorption/desorption between the solid and dissolved phases is extremely fast ($a_i^{1,2}$, Table 1). Therefore the pertinent factors affecting the dissolved ^{137}Cs concentrations are K_d, the soil particle size distribution, and the concentration of ^{137}Cs in the soil particles, which in turn depends on the ^{137}Cs inventory. For the surface cells, again the extremely fast rate of absorption and desorption means equilibrium between the dissolved and particulate phases is attained almost immediately in the simulations. The important factors

339 controlling the dissolved ^{137}Cs concentration are therefore the K_d values, the suspended
340 sediment size distribution, the quantity of suspended sediment and the inflow of dissolved ^{137}Cs
341 and particulates. The latter two factors distinguish the dissolved ^{137}Cs behavior in surface cells
342 from the subsurface cells. Inflow/outflow has only a small effect for the subsurface cells due to
343 the much larger inventory of ^{137}Cs present in the soil. Inflow/outflow however has a large
344 bearing for the surface cells due to the balance of between dissolved ^{137}Cs concentrations and
345 suspended sediment ^{137}Cs concentrations set by K_d.

346 For the case 1 simulation, K_d was identical for all particle grades up to 0.3 mm
347 representative diameter (Table 1). For case 2 however, K_d varied between the finer 0.001 and
348 0.01 mm and the larger 0.1 and 0.3 mm sediment grades. The results show that the dissolved
349 ^{137}Cs concentrations in river water (surface cells) are close to the mean dissolved ^{137}Cs
350 concentrations in pore water in neighboring subsurface cells as shown in Fig. 8(a). Therefore
351 transported suspended sediments during base-flow periods only have a small influence on the
352 variation of dissolved ^{137}Cs concentrations.

353 The dissolved ^{137}Cs concentrations in the outflow river were higher in the case 2 simulation
354 than the case 1 simulation because of the higher dissolved ^{137}Cs concentrations in pore water.
355 This was in turn due to the lower affinity for the larger 0.1 and 0.3 mm sediment grades to bind
356 ^{137}Cs (as set by the K_d values) than for the case 1 simulation.

357 In spite of the fact that the simulations reproduced the water discharge, suspended
358 sediment flux and particulate ^{137}Cs concentrations reasonably well, both the case 1 and 2
359 simulations did not yield peaks in dissolved ^{137}Cs concentrations over Typhoons Phanfone,
360 Vongfong, and Nangka. Likewise the simulations did not show any seasonal variation of the
361 dissolved ^{137}Cs concentrations at the catchment outlet. In the GETFLOWS simulations,
362 hydrological factors, such as the amount of precipitation, evapo-transpiration, water discharge,
363 and the height of the water table, have a smaller effect on dissolved ^{137}Cs concentrations in river

364 water than on particulate ^{137}Cs concentrations. High precipitation in summer causes the
365 transport of large amounts of sediment by rivers, particularly during typhoons. This may
366 influence the dissolved ^{137}Cs concentration in river water through desorption or adsorption, but
367 not by enough to explain the peaks in dissolved ^{137}Cs concentrations that occurred during storms.
368 There may be an attenuation effect of larger water discharge rates diluting the dissolved
369 substances (Muraoka and Hirata, 1988) or increased amounts of adsorption due to the higher
370 suspended sediment loads in the simulations (Fig. 7). However Tsuji et al. (2016) reported that
371 suspended solids and dissolved ^{137}Cs concentrations are correlated under both base and storm
372 flow conditions.

373 The assumed fast rate of absorption/desorption (Table 1) may be a limitation of the model.
374 Yoshimura et al. (2015b) suggested that particulate and dissolved ^{137}Cs concentrations in field
375 samples may not reach equilibrium. The effects of coexisting ions (Tsuji et al., 2016) or mineral
376 composition (Cha et al., 2006) of suspended sediments in river water are not captured by the
377 simple K_d model employed in this study. Moreover K_d itself may vary between the environments
378 of river water, riverbeds and forests due to variations in the particle size distribution. The
379 distribution coefficient has also been suggested to vary with organic matter content (Valcke and
380 Cremers, 1994). However even by varying the K_d values in the GETFLOWS simulation model,
381 it would be difficult to reproduce the peaks in dissolved ^{137}Cs concentrations in storms, and
382 seasonal variability of base flow levels.

383 The simulations did not model the organic matter layer in the catchment's forests. During
384 storm periods, saturation of the ground leads to large amounts of surface run-off through forest
385 litter layers. Cesium-137 may leach from the organic matter in these conditions, and then flow
386 into rivers (Tsuji et al., 2016). Obvious candidates for explaining seasonal variation are
387 biological factors. Microbial activity varies with atmospheric temperature and litter layer mass
388 also has a seasonal dependence. It is necessary to include a litter layer explicitly in the

389 simulations to gauge the possible extent of these factors on dissolved ^{137}Cs concentrations.

390 **4.2 Sources of dissolved ^{137}Cs**

391 Dissolved ^{137}Cs concentrations in pore water are almost always constant due to the fast
392 rate of absorption and desorption between the bound and dissolved phases in the GETFLOWS
393 model. There is a small amount of variation of the dissolved ^{137}Cs concentration in pore water
394 between locations across the study area (Fig. 8(a), as discussed in section 4.1). This is a
395 consequence of different soil particle size distributions and ^{137}Cs inventories. Locations at high
396 altitudes tend to have large inventories due to the characteristics of the fallout distribution
397 (Fig. 1).

398 In the GETFLOWS simulations, pore water contributes dissolved ^{137}Cs to the surface
399 water flows where springs discharge through the surface. The spatial distribution of dissolved
400 ^{137}Cs concentrations in river water under base flow conditions is shown in Fig. 8(b). The grid
401 resolution of the simulations (approximately 40 m) is large compared to the width of mountain
402 streams in reality (approximately 1-5 m).

403 Under storm flow conditions, surface water flows gradually cover more of the catchment
404 area (Fig. 8(c) and (d)). The flows first cover the riparian zones (Fig. 8(c)) followed by the
405 filling of mountain streams that are normally dry in base flow periods (Fig. 8(d)). These two
406 areas are the main sources of the dissolved ^{137}Cs carried in flood waters during storms. The
407 higher water discharge rates that occur during storms attenuate dissolved ^{137}Cs concentrations,
408 despite the additional input of dissolved ^{137}Cs from the riparian zones and mountain streams.
409 This means peaks are not seen in the dissolved ^{137}Cs concentrations over storm periods (Fig. 7).

410 Additional processes not captured in our simulations could contribute to dissolved ^{137}Cs
411 input to rivers during storms. Cesium-137 may leach from litter accumulated in the riparian
412 zones, as microbial and mechanical decomposition is assisted by flooding. It is useful
413 nonetheless to have predictions for where surface water flows occurs, as this information can

414 be used to plan environmental countermeasures, e.g. the removal of litter to prevent leaching
415 and ^{137}Cs entering rivers.

416 Tegen and Dörr (1996), Nakanishi et al. (2014) and Koarashi et al. (2016) found that ^{137}Cs
417 rapidly leaches from forest floor litter, and that the downward migration of ^{137}Cs in forest soil
418 is faster during the summer season than in winter. Murakami et al. (2014) and Sakai et al. (2016)
419 noted that there are generally much lower ^{137}Cs concentrations in stream litter than forest litter.
420 Cesium-137 leaching from organic matter may therefore be an important factor in determining
421 ^{137}Cs concentrations in river water, although currently there is insufficient understanding of the
422 connectivity between the riparian zone and rivers to make a firm conclusion.

423 **5. Conclusion**

424 Watershed simulations and field monitoring results were combined to investigate the
425 applicability of the K_d absorption/desorption model for simulating dissolved ^{137}Cs
426 concentrations in river water within a forested catchment in Fukushima Prefecture. The
427 simulations reproduced mean concentrations of dissolved ^{137}Cs at the catchment outlet during
428 base flow periods. However the simulations were unsuccessful in reproducing the peaks in
429 dissolved ^{137}Cs concentrations during storms and the seasonal variability shown under base
430 flow conditions. Leaching of ^{137}Cs from organic matter in forest litter layers, which was not
431 modeled in the simulations, may explain the discrepancy between the simulations and field
432 observations.

433 Watershed modeling can be used to interpret dissolved ^{137}Cs concentrations observed in
434 field monitoring studies. A benefit of 2D and 3D codes over 1D codes is the ability to spatially
435 resolve ^{137}Cs redistribution across the catchment. Areas making a high contribution to ^{137}Cs
436 input to watercourses, and areas where ^{137}Cs accumulates due to deposition, can be identified
437 and countermeasures effected as necessary. The results of this study suggest however that code
438 developments are warranted to improve simulation results for dissolved ^{137}Cs concentrations in

439 Fukushima watersheds, such as modeling of ^{137}Cs leaching from organic litter layers in forests
440 or refinements to the K_d absorption/desorption model.

441 **Acknowledgements**

442 We thank members of the Fukushima Environmental Safety Center and the Center for
443 Computational Science & e-Systems for their support to this research, and in particular Takahiro
444 Nakanishi for him comments on the manuscript. We also thank the staff at Geosphere
445 Environmental Technology Corporation for their assistance on operating GETFLOWS.

446 **References**

447 Cha, H.J., Kang, M.J., Geun, H.C., Geun, S.C., Chang, W.L., 2006. Accumulation of ^{137}Cs in
448 soils on different bedrock geology and textures. J. Radioanal. Nucl. Chem. 267, 349-355.
449 doi:10.1007/s10967-006-0054-4
450 Evrard, O., Chartin, C., Onda, Y., Lepage, H., Cerdan, O., Lefèvre, I., Ayrault, S., 2014.
451 Renewed soil erosion and remobilisation of radioactive sediment in Fukushima coastal rivers
452 after the 2013 typhoons. Sci. Rep. 4, 4574. doi:10.1038/srep04574
453 Evrard, O., Laceby, J., Lepage, H., Onda., Y., Cerdan, O., Ayrault, S., 2015. Radiocesium
454 transfer from hillslopes to the Pacific Ocean after the Fukushima Nuclear Power Plant
455 accident: a review. J. Environ. Radioact. 148, 92-110. doi:10.1016/j.jenvrad.2015.06.018
456 Eyrolle-Boyer, F., Boyer, P., Garcia-Sanchez, L., Métivier, J.M., Onda, Y., De Vismes, A.,
457 Cagnat, X., Boulet, B., Cossonnet, C., 2016. Behaviour of radiocaesium in coastal rivers of
458 the Fukushima Prefecture (Japan) during conditions of low flow and low turbidity - Insight
459 on the possible role of small particles and detrital organic compounds. J. Environ. Radioact.
460 151, 328–340. doi:10.1016/j.jenvrad.2015.10.028
461 Geological Survey of Japan. 2012. [Available at https://www.gsj.jp/en/index.html, Accessed 9
462 March 2015.]

Geospatial Information Authority of Japan. 2012. [Available at http://www.gsi.go.jp/ENGLISH/, Accessed 9 March 2015.]

Hamon, W.R., 1961. Estimating potential evapotranspiration, Proceedings American Society of Civil Engineers. 87(HY 3), 107-120.

He, Q., Walling, D.E., 1996. Interpreting particle size effects in the adsorption of ^{137}Cs and unsupported ^{210}Pb by mineral soils and sediments. J. Environ. Radioact. 30, 117-137. doi:10.1016/0265-931X(96)89275-7

Iwagami, S., Onda, Y., Tsujimura, M., Abe, Y., 2016. Contribution of radioactive ^{137}Cs discharge by suspended sediment, coarse organic matter, and dissolved fraction from a headwater catchment in Fukushima after the Fukushima Dai-ichi Nuclear Power Plant accident. J. Environ. Radioact. doi:10.1016/j.jenvrad.2016.07.025

Japan Meteorological Agency (JMA), 2014 and 2015. AMeDAS Data (in Japanese).

Kitamura, A., Kurikami, H., Sakuma, K., Malins, A., Okumura, M., Machida, M., Mori, K., Tada, K., Tawara, Y., Kobayashi, T., Yoshida, T., Tosaka, H., 2016. Redistribution and export of contaminated sediment within eastern Fukushima Prefecture due to typhoon flooding. Earth Surf. Process. Landforms 1726, 1708–1726. doi:10.1002/esp.3944

Koarashi, J., Nishimura, S., Nakanishi, T., Atarashi-Andoh, M., Takeuchi, E., Muto, K., 2016. Post-deposition early-phase migration and retention behavior of radiocesium in a litter-mineral soil system in a Japanese deciduous forest affected by the Fukushima nuclear accident. Chemosphere 165, 335-341. doi:10.1016/j.chemosphere.2016.09.043

Kurikami, H., Kitamura, A., Yokuda, S.T., Onishi, Y., 2014. Sediment and ^{137}Cs behaviors in the Ogaki Dam Reservoir during a heavy rainfall event. J. Environ. Radioact. 137, 10-17. doi:10.1016/j.jenvrad.2014.06.013

Kurikami, H., Funaki, H., Malins, A., Kitamura, A., Onishi, Y., 2016. Numerical study of sediment and ^{137}Cs discharge out of reservoirs during various scale rainfall events. J. Environ.

Radioact. 164, 73-83. doi:10.1016/j.jenvrad.2016.07.004

Livens, F.R., Baxter, M.S., 1988. Particle size and radionuclide levels in some west Cumbrian soils. Sci. Total Environ. 70, 1-17. doi:10.1016/0048-9697(88)90248-3

Malins, A., Kurikami, H., Nakama, S., Saito, T., Okumura, M., Machida, M., Kitamura, A., 2016. Evaluation of ambient dose equivalent rates influenced by vertical and horizontal distribution of radioactive cesium in soil in Fukushima Prefecture. J. Environ. Radioact. 151, 38-49. doi:10.1016/j.jenvrad.2015.09.014

Ministry of Agriculture, Forestry and Fisheries, 2015. [Available at http://www.rinya.maff.go.jp/j/press/kaihatu/pdf/150327-01.pdf, Accessed 10 February 2017.]

Ministry of Economy, Trade and Industry, 2017. [Available at http://www.meti.go.jp/english/earthquake/nuclear/roadmap/pdf/gainenzu_201704e.pdf, Accessed 14 November 2017.]

Ministry of Education, Culture, Sports, Science and Technology, 2011. Results of the Third Airborne Monitoring Survey by MEXT. [Available at http://www.mext.go.jp/component/english/__icsFiles/afieldfile/2011/07/22/1304797_0708e.pdf, Accessed 24 November 2016.]

Ministry of Land, Information, Transport and Tourism, 2016. [Available at http://nrb-www.mlit.go.jp/kokjo/inspect/landclassification/land/20-1/07.html, Accessed 29 March 2017 (in Japanese).]

Ministry of the Environment, 2016. Natural environmental information GIS. [Available at http://www.biodic.go.jp/trialSystem/top_en.html, Accessed 4 November 2016.]

Monte, L., 2014. Application of the migration models implemented in the decision system MOIRA-PLUS to assess the long term behaviour of ^{137}Cs in water and fish of the Baltic Sea. J. Environ. Radioact. 134, 136-144. doi:10.1016/j.jenvrad.2014.03.009

513 Mori, K., Tada, K., Tawara, Y., Ohno, K., Asami, M., Kosaka, K., Tosaka, H., 2015. Integrated
514 watershed modeling for simulation of spatiotemporal redistribution of post-fallout
515 radionuclides: Application in radiocesium fate and transport processes derived from the
516 Fukushima accidents. Environ. Model. Softw. 72, 126–146.
517 doi:10.1016/j.envsoft.2015.06.012
518 Murakami, M., Ohte, N., Suzuki, T., Ishii, N., Igarashi, Y., Tanoi, K., 2014. Biological
519 proliferation of cesium-137 through the detrital food chain in a forest ecosystem in Japan.
520 Sci. Rep. 4, 3599. doi:10.1038/srep03599
521 Muraoka, K., Hirata, T., 1988. Streamwater chemistry during rainfall events in a forested basin.
522 J. Hydrol. 102, 235-253. doi:10.1016/0022-1694(88)90100-X
523 Nagao, S., Kanamori, M., Ochiai, S., Tomihara, S., Fukushi, K., Yamamoto, M., 2013. Export
524 of ^{134}Cs and^{137}Cs in the Fukushima river systems at heavy rains by Typhoon Roke in
525 September 2011. Biogeosciences 10, 6215–6223. doi:10.5194/bg-10-6215-2013
526 Nagao, S., Kanamori, M., Ochiai, S., Inoue, M., Yamamoto, M., 2015. Migration behavior of
527 ^{134}Cs and ^{137}Cs in the Niida River water in Fukushima Prefecture, Japan during 2011-2012.
528 J. Radioanal. Nucl. Chem. 303, 1617-1621. doi:10.1007/s10967-014-3686-9
529 Nakanishi, T.M., Kobayashi, N.I., Tanoi, K., 2013. Radioactive cesium deposition on rice,
530 wheat, peach tree and soil after nuclear accident in Fukushima. J. Radioanal. Nucl. Chem.
531 296, 985-989. doi:10.1007/s10967-012-2154-7
532 Nakanishi, T., Matsunaga, T., Koarashi, J., Atarashi-Andoh, M., 2014. ^{137}Cs vertical migration
533 in a deciduous forest soil following the Fukushima Dai-ichi Nuclear Power Plant accident. J.
534 Environ. Radioact. 128, 9-14. doi:10.1016/j.jenvrad.2013.10.019
535 National Institute of Advanced Science and Technology, 2016. GeomapNavi. [Available at
536 https://gbank.gsj.jp/geonavi/?lang=en, Accessed 14 November 2017.]
537 Niizato, T., Abe, H., Mitachi, K., Sasaki, Y., Ishii, Y., Watanabe, T., 2016. Input and output

budgets of radiocesium concerning the forest floor in the mountain forest of Fukushima released from the TEPCO's Fukushima Dai-ichi nuclear power plant accident. J. Environ. Radioact. 161, 11-21. doi:10.1016/j.jenvrad.2016.04.017

Nylén, T., Grip, H., 1997. The origin and dynamics of ^{137}Cs discharge from a coniferous forest catchment. J. Hydrol. 192, 338-354. doi:10.1016/S0022-1694(96)03083-1

Ochiai, S., Ueda, S., Hasegawa, H., Kakiuchi, H., Akata, N., Ohtsuka, Y., Hisamatsu, S., 2015. Effects of radiocesium inventory on ^{137}Cs concentrations in river waters of Fukushima, Japan, under base-flow conditions. J. Environ. Radioact. 144, 86–95. doi:10.1016/j.jenvrad.2015.03.005

Onishi, Y., Voitsekhovich, O.V., Zheleznyak, M.J., 2007. Chernobyl – What Have We Learned? Springer. ISBN: 978-1-4020-5348-1

Saito, K. and Petoussi-Henss N., 2014. Ambient dose equivalent conversion coefficients for radionuclides exponentially distributed in the ground. J. Nucl. Sci. Technol. 51, 1274-1287. doi:10.1080/00223131.2014.919885

Saito, K., Tanihata, I., Fujiwara, M., Saito, T., Shimoura, S., Otsuka, T., Onda, Y., Hoshi, M., Ikeuchi, Y., Takahashi, F., Kinouchi, N., Saegusa, J., Seki, A., Takemiya, H., Shibata, T., 2015. Detailed deposition density maps constructed by large-scale soil sampling for gamma-ray emitting radioactive nuclides from the Fukushima Dai-ichi Nuclear Power Plant accident. J. Environ. Radioact. 139, 308-319. doi:10.1016/j.jenvrad.2014.02.014

Sakaguchi, A., Tanaka, K., Iwatani, H., Chiga, H., Fan, Q., Onda, Y., Takahashi, Y., 2015. Size distribution studies of ^{137}Cs in river water in the Abukuma Riverine system following the Fukushima Dai-ichi Nuclear Power Plant accident. J. Environ. Radioact. 139, 379-389. doi:10.1016/j.jenvrad.2014.05.011

Sakai, M., Gomi, T., Negishi, J.N., 2016. Fallout volume and litter type affect ^{137}Cs concentration difference in litter between forest and stream environments. J. Environ.

563 Radioact. 164, 169-173. doi:10.1016/j.jenvrad.2016.07.030
564 Sakuma, K., Kitamura, A., Malins, A., Kurikami, H., Machida, M., Mori, K., Tada, K.,
565 Kobayashi, T., Tawara, Y., Tosaka, H., 2017. Characteristics of radio-cesium transport and
566 discharge between different basins near to the Fukushima Dai-ichi Nuclear Power Plant after
567 heavy rainfall events. J. Environ. Radioact. 169-170, 130–150.
568 doi:10.1016/j.jenvrad.2016.12.006
569 Sakuma, K., Malins, A., Funaki, H., Kurikami, H., Niizato, T., Nakanishi, T., Mori, K., Tada,
570 K., Kobayashi, T., Kitamura, A., Hosomi, M., 2018. Evaluation of sediment and ^{137}Cs
571 redistribution in the Oginosawa River catchment near the Fukushima Dai-ichi Nuclear Power
572 Plant using integrated watershed modeling. J. Environ. Radioact. 182, 44-51.
573 doi:10.1016/j.jenvrad.2017.11.021
574 Shinomiya, Y., Tamai, K., Kobayashi, M., Ohnuki, Y., Shimizu, T., Iida, S., Nobuhiro, T.,
575 Sawano, S., Tsuboyama, Y., Hiruta, T., 2014. Radioactive cesium discharge in stream water
576 from a small watershed in forested headwaters during a typhoon flood event. Soil Sci. Plant
577 Nutr. 60, 765–771. doi:10.1080/00380768.2014.949852
578 Takada, M., Yamada, T., Takahara, T., Endo, S., Tanaka, K., Kajimoto, T., Okuda, T., 2017.
579 Temporal changes in vertical distribution of ^{137}Cs in litter and soils in mixed deciduous
580 forests in Fukushima, Japan. J. Nucl. Sci. Technol. 54, 452-458.
581 doi:10.1080/00223131.2017.1287602
582 Tegen, I., Dörr, H., 1996. Mobilization of cesium in organic rich soils: Correlation with
583 production of dissolved organic carbon. Water Air Soil Pollut. 88, 133-144.
584 doi:10.1007/BF00157418
585 Tsuji, H., Yasutaka, T., Kawabe, Y., Onishi, T., Komai, T., 2014a. Distribution of dissolved and
586 particulate radiocesium concentrations along rivers and the relations between radiocesium
587 concentration and deposition after the nuclear power plant accident in Fukushima. Water Res.

60, 15–27. doi:10.1016/j.watres.2014.04.024

Tsuji, H., Kondo, Y., Kawashima, S., Yasutaka, T., 2014b. Non-destructive detection of particulate radiocesium using a non-woven fabric cartridge filter for rapid preprocessing. J. Radioanal. Nucl. Chem. 300, 1803-1810. doi:10.1007/s10967-014-3800-z

Tsuji, H., Nishikiori, T., Yasutaka, T., Watanabe, M., Ito, S., Hayashi, S., 2016. Behavior of dissolved radiocesium in river water in a forested watershed in Fukushima Prefecture. J. Geophys. Res.: Biogeosciences 121, 2588-2599. doi:10.1002/2016JG003428

Ueda, S., Hasegawa, H., Kakiuchi, H., Akata, N., Ohtsuka, Y., Hisamatsu, S., 2013. Fluvial discharges of radiocaesium from watersheds contaminated by the Fukushima Dai-ichi Nuclear Power Plant accident, Japan. J. Environ. Radioact. 118, 96–104. doi:10.1016/j.jenvrad.2012.11.009

Uematsu, S., Vandenhove, H., Sweeck, L., Hees, M.V., Wannijn, J., Smolders, E., 2017. Foliar uptake of radiocaesium from irrigation water by paddy rice (Oryza sativa): an overlooked pathway in contaminated environments. New Phytol. 214, 820-829. doi:10.1111/nph.14416

Valcke, E., Cremers, A., 1994. Sorption-desorption dynamics of radiocaesium in organic matter soils. Sci. Total Environ. 157, 275-283. doi:10.1016/0048-9697(94)90590-8

Yamashiki, Y., Onda, Y., Smith, H.G., Blake, W.H., Wakahara, T., Igarashi, Y., Matsuura, Y., Yoshimura, K., 2014. Initial flux of sediment-associated radiocesium to the ocean from the largest river impacted by Fukushima Daiichi Nuclear Power Plant. Sci. Rep. 4, 3714. doi:10.1038/srep03714

Yasutaka, T., Tsuji, H., Kondo, Y., Suzuki, Y., Takahashi, A., Kawamoto, T., 2015. Rapid quantification of radiocesium dissolved in water by using nonwoven fabric cartridge filters impregnated with potassium zinc ferrocyanide. J. Nucl. Sci. Technol. 52, 792-800. doi:10.1080/00223131.2015.1013071

Yoschenko, V., Takase, T., Konoplev, A., Nanba, K., Onda, Y., Kivva, S., Zheleznyak, M., Sato,

N., Keitoku, K., 2017. Radiocesium distribution and fluxes in the typical Cryptomeria japonica forest at the late stage after the accident at Fukushima Dai-Ichi Nuclear Power Plant. J. Environ. Radioact. 166, 45-55. doi:10.1016/j.jenvrad.2016.02.017

Yoshikawa, N., Obara, H., Ogasa, M., Miyazu, S., Harada, N., Nonaka, M., 2014. ^{137}Cs in irrigation water and its effect on paddy fields in Japan after the Fukushima nuclear accident, Sci. Total Environ. 481, 252–259. doi:10.1016/j.scitotenv.2014.01.129

Yoshimura, K., Onda, Y., Kato, H., 2015a. Evaluation of radiocaesium wash-off by soil erosion from various land uses using USLE plots. J. Environ. Radioact. 139, 362-369. doi:10.1016/j.jenvrad.2014.07.019

Yoshimura, K., Onda, Y., Sakaguchi, A., Yamamoto, M., Matsuura, Y., 2015b. An extensive study of the concentrations of particulate/dissolved radiocaesium derived from the Fukushima Dai-ichi Nuclear Power Plant accident in various river systems and their relationship with catchment inventory. J. Environ. Radioact. 139, 370–378. doi:10.1016/j.jenvrad.2014.08.021

Zheleznyak, M.J., Demchenko, R.I., Khursin, S.L., Kuzmenko, Y.I., Tkalich, P.V., Vitiuk, N.Y., 1992. Mathematical modeling of radionuclide dispersion in the Pripyat-Dnieper aquatic system after the Chernobyl accident. Sci.Total.Environ. 112, 89-114. doi:10.1016/0048-9697(92)90241-J

Figure captions

Fig. 1 Map showing upstream Ota River catchment (black hatched area) within the full Ota River basin (shown by thick black boundary line), and proximity to the FDNPP site. Colors depict ^{137}Cs inventory in July 2011.

Fig. 2 Three dimensional hydrogeological structure model of the study area. Colors indicate different deposits and bedrock types (individually labelled).

Fig. 3 Simulated and measured hourly mean water discharge rates at the catchment outlet over the full two year study period, along with hourly precipitation rates.

Fig. 4 Simulated and measured hourly mean suspended sediment fluxes at the catchment outlet between 29 May 2014 and 10 Sep 2015.

Fig. 5 Simulated and measured river water discharge rates (upper panels) and suspended sediment fluxes (lower panels) at the catchment outlet over the periods of Typhoons Phanfone (5-10 October 2014), Vongfong (13-18 October 2014), and Nangka (15-20 June 2015). Upper panels also show precipitation rates over the storms.

Fig. 6 Results for dissolved and particulate ^{137}Cs concentrations in the catchment outflow.

Fig. 7 Comparison of simulated and measured dissolved ^{137}Cs concentrations under storm flow conditions in the catchment outflow.

Fig. 8 Spatial distribution of dissolved ^{137}Cs concentration (a) in the pore water in surface soil and (b) – (d) in the surface water before and during 16 July 2015 (Typhoon Nangka) for simulation case 1 (case 2 simulation shows similar trends).

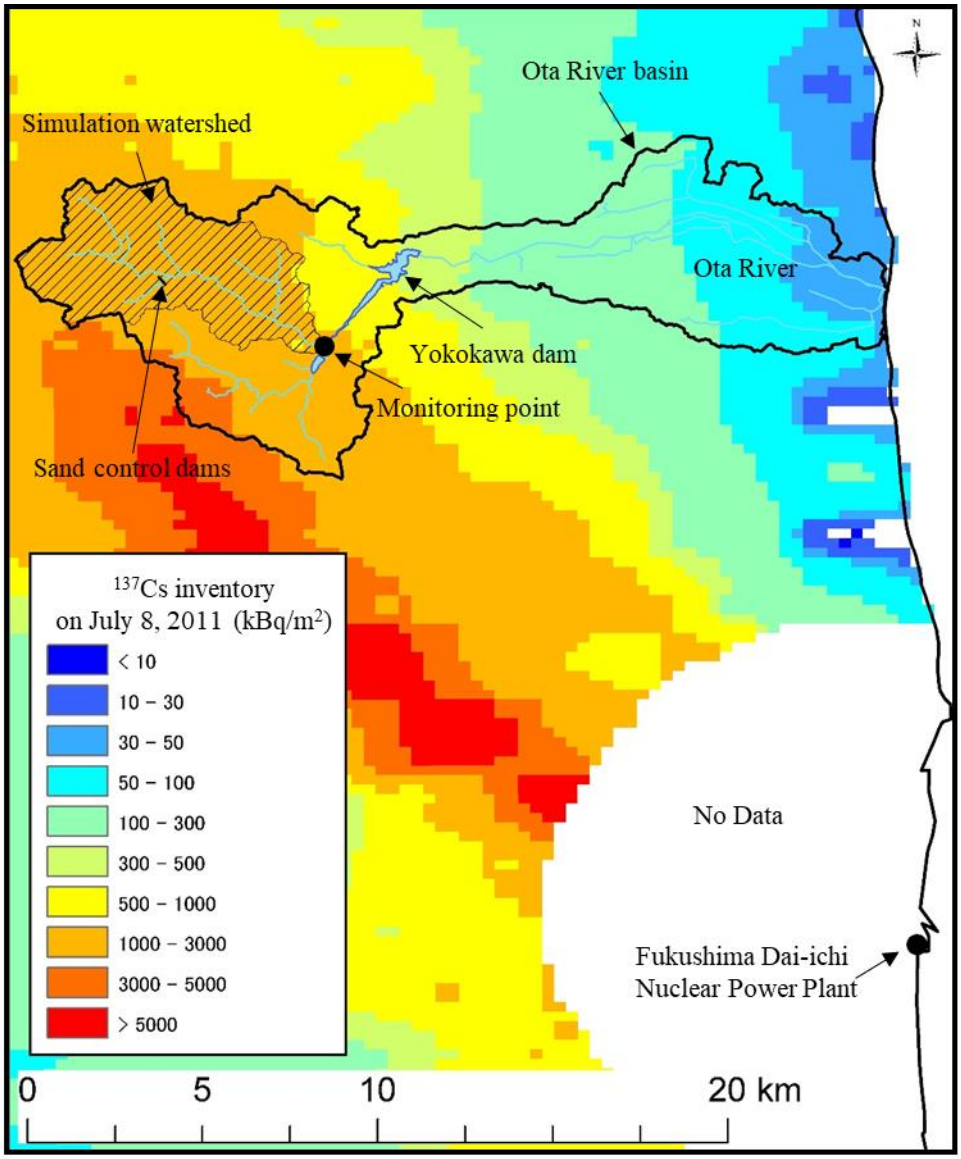
Ota River basin
Simulation watershed
Ota River
Yokokawa dam
Monitoring point
Sand control dams
137Cs inventory
on July 8, 2011 (kBq/m2)
< 10
10 – 30
30 – 50
50 – 100
100 – 300
300 – 500
500 – 1000
1000 – 3000
3000 – 5000
> 5000
No Data
Fukushima Dai-ichi
Nuclear Power Plant
0
5
10
20 km

652

653 Fig. 1

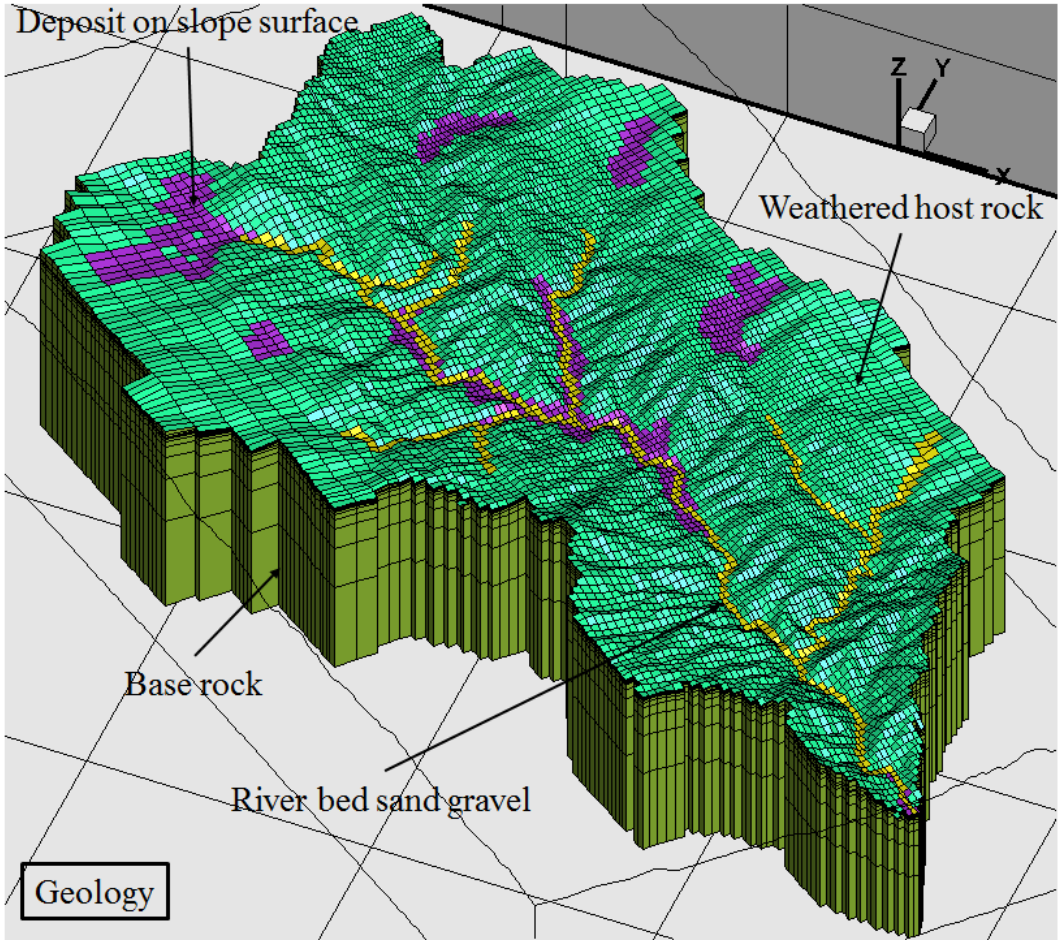
Deposit on slope surface
Z
Y
X
Weathered host rock
Base rock
River bed sand gravel
Geology

Fig. 2

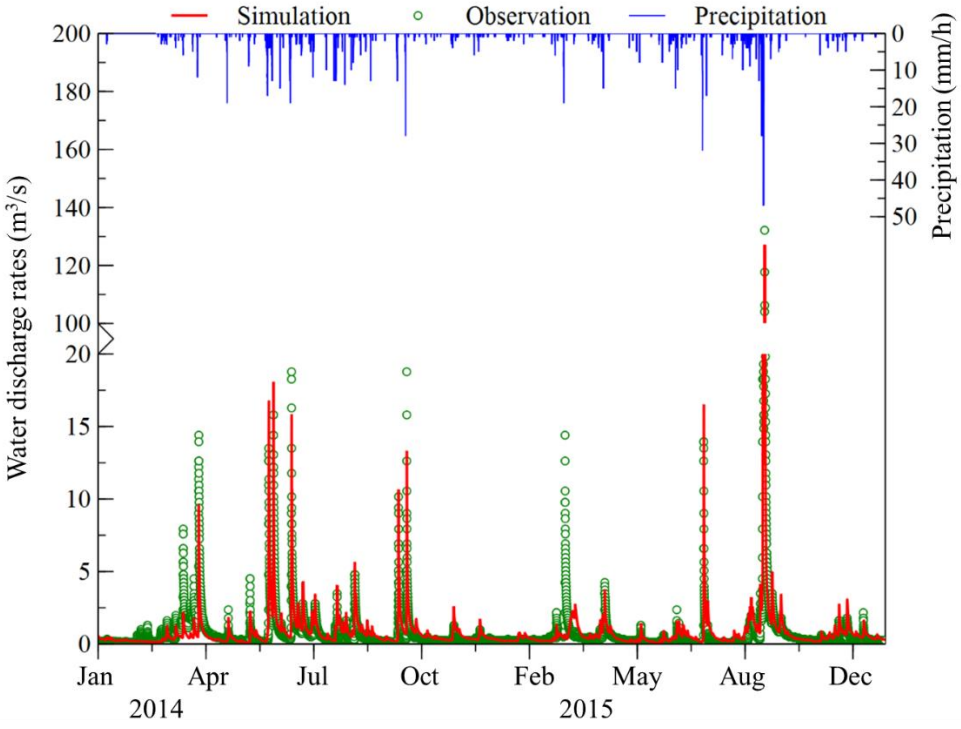
Simulation
Observation
Precipitation
Water discharge rates (m³/s)
Precipitation (mm/h)
200
180
160
140
120
100
20
15
10
5
0
0
10
20
30
40
50
Jan
Apr
Jul
Oct
Feb
May
Aug
Dec
2014
2015

Fig. 3

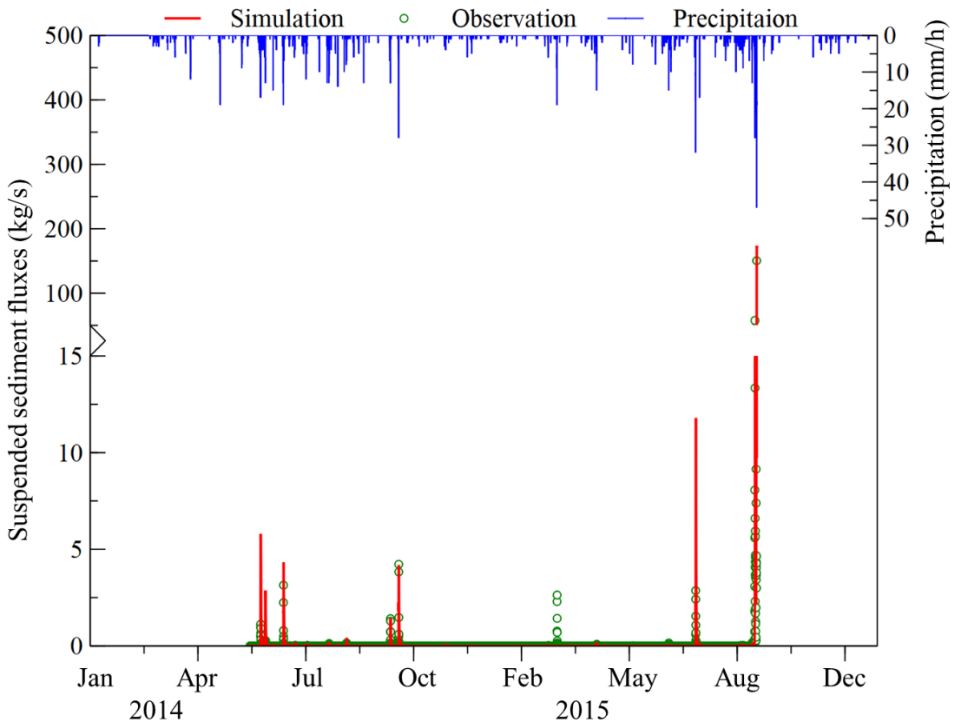

658

659 Fig. 4

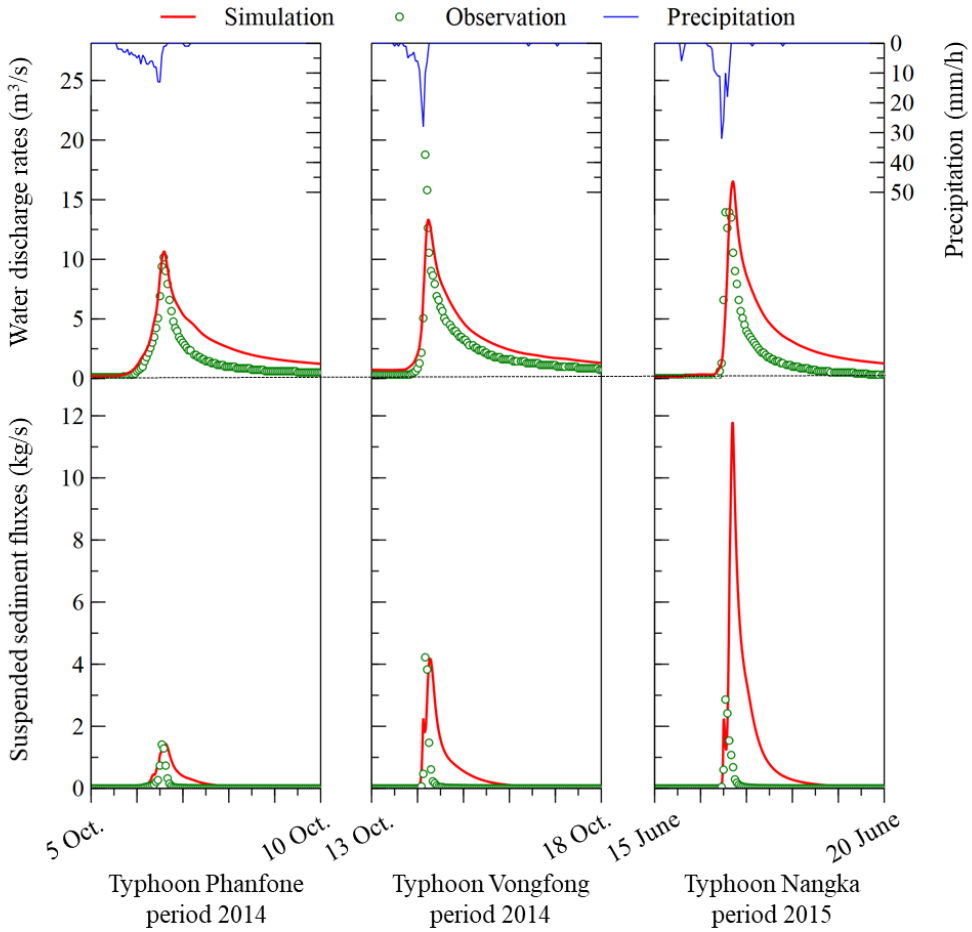

660

661 Fig. 5

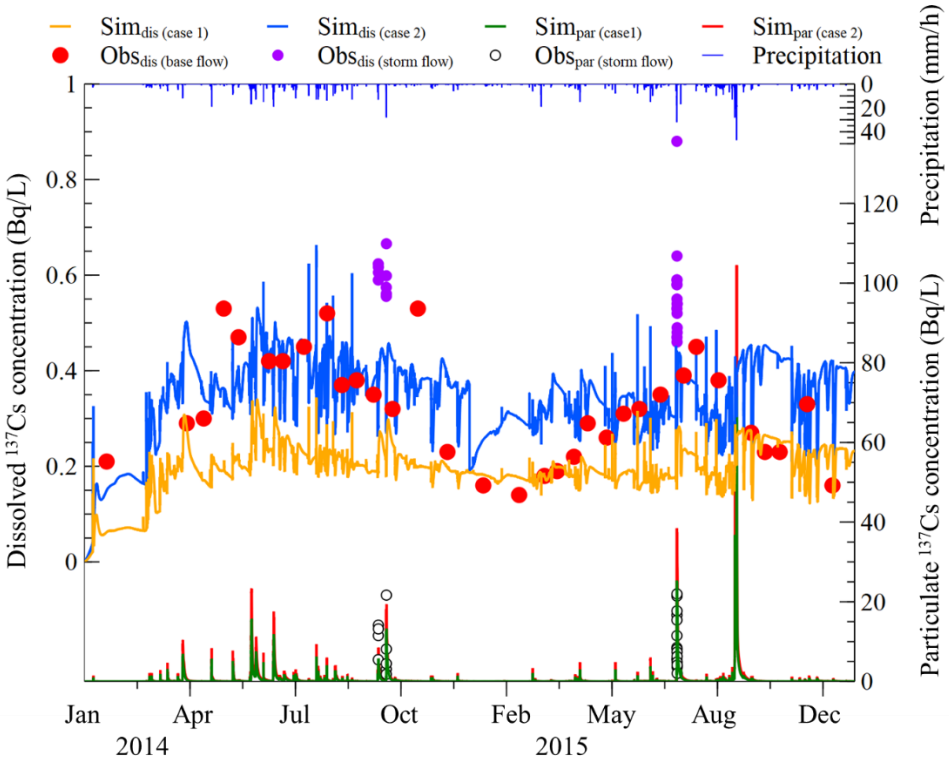
Sim dis (case 1)
Obs dis (base flow)
Sim dis (case 2)
Obs dis (storm flow)
Sim par (case1)
Obs par (storm flow)
Sim par (case 2)
Precipitation
Dissolved 137Cs concentration (Bq/L)
Particulate 137Cs concentration (Bq/L)
Precipitation (mm/h)
Jan
Apr
Jul
Oct
Feb
May
Aug
Dec
2014
2015

662

663 Fig. 6

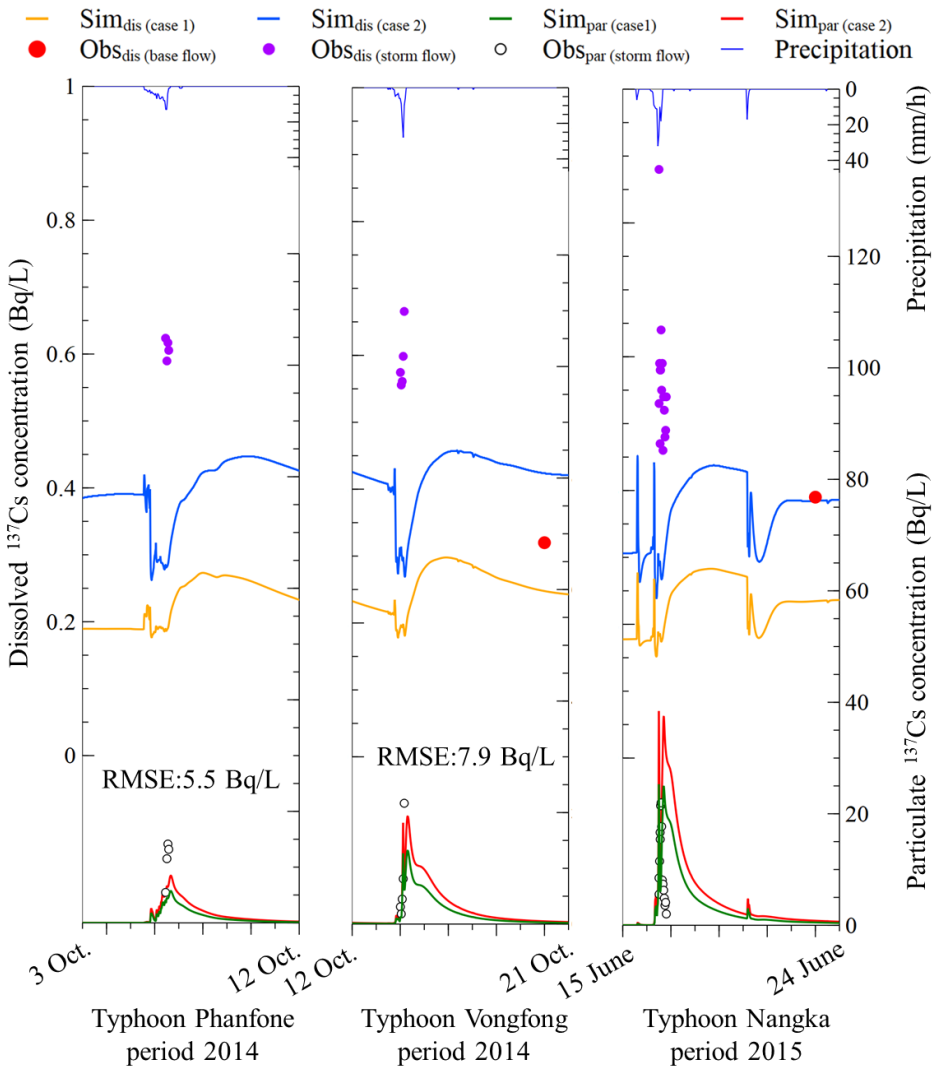
Sim dis (case 1)
Obs dis (base flow)
Sim dis (case 2)
Obs dis (storm flow)
Sim par (case1)
Obs par (storm flow)
Sim par (case 2)
Precipitation
Dissolved 137Cs concentration (Bq/L)
Particulate 137Cs concentration (Bq/L)
Precipitation (mm/h)
RMSE:5.5 Bq/L
RMSE:7.9 Bq/L
3 Oct.
12 Oct.
12 Oct.
21 Oct.
15 June
24 June
Typhoon Phanfone period 2014
Typhoon Vongfong period 2014
Typhoon Nangka period 2015

664

665 Fig. 7

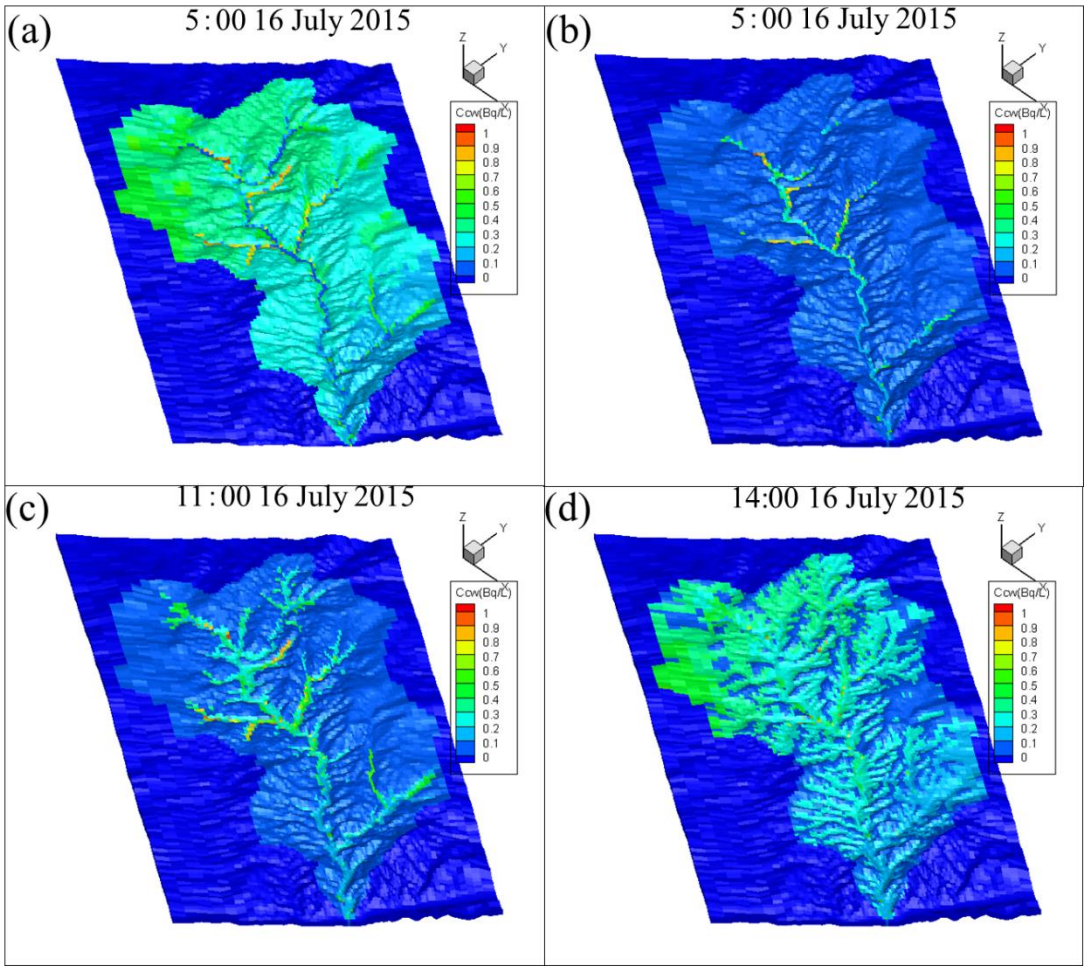
(a)
5:00 16 July 2015
(b)
5:00 16 July 2015
(c)
11:00 16 July 2015
(d)
14:00 16 July 2015
Ccw(Bq/L)
1
0.9
0.8
0.7
0.6
0.5
0.4
0.3
0.2
0.1
0
Z
Y
X

Fig. 8

668 Table 1. ^{137}Cs transport parameters.

	Unit	Grain size (mm)	Case 1	Case 2
Molecular diffusion coefficient	m^2/s	-	2.1×10^{-9}	2.1×10^{-9}
Tortuosity factor	-	-	0.5	0.5
Dispersion length	m	-	0.1 (Vertical), 0.01 (Horizontal)	0.1 (Vertical), 0.01 (Horizontal)
a_i[1,2]	s^{-1}	All grades	1.2	1.2
Distribution coefficient K_d	L/kg	0.001	2.0×10^5	2.0×10^5
		0.01	2.0×10^5	2.0×10^5
		0.1	2.0×10^5	5.0×10^4
		0.3	2.0×10^5	5.0×10^4
		1	0	0
		5	0	0

669 Table 2. Total ^{137}Cs discharge from catchment between 29 May 2014 and 29 May 2015.

Case	Dissolved (Bq)		Particulate (Bq)	
	Simulation	Observation[a]	Simulation	Observation[a]
Case 1	4.0×10^9	8.7×10^9	4.8×10^{10}	2.1×10^{10}
Case 2	7.9×10^9		7.3×10^{10}	

670 [a] Tsuji et al. (2016).

Supplementary Material to Applicability of K_d for modelling dissolved ^{137}Cs concentrations in Fukushima river water: case study of the upstream Ota River

The various input parameters used in this simulations are given in Tables S1 to S6. Table S1 lists Manning's roughness coefficient for each land use and vegetation. Table S2 lists raindrop-induced erosion parameters depending on land use and vegetation. Table S3 and S4 list hydraulic parameters for grid-blocks in the surface soil and subsurface layers, these parameters were calibrated using hydrographs based on observation data. Table S5 lists sediment particle size distribution. We modeled six representative particle diameters of 0.001, 0.01, 0.1, 0.3, 1 and 5 mm, respectively. Although radiocesium is strongly adsorbed by the fine particle grades, it is necessary to model all grades to calculate radiocesium concentrations within sediments. Table S6 lists soil detachment properties due to a raindrops and surface water flow (Morgan et al., 1998). Numbers highlighted with bold font in Tables S4 to S6 indicate parameters that were tuned in this study, i.e. parameters different from previous Sakuma et al. (2017, 2018) studies.

Table S7 lists the measurements of dissolved ^{137}Cs concentration in river water at the catchment outlet taken subsequent to the Tsuji et al. (2016) study. Table S8 lists statistics for the correlation between measured and simulated dissolved ^{137}Cs concentrations in the river water at the catchment outlet under base flow conditions. Figure S1 shows the correspondence between the dissolved ^{137}Cs measurements and the simulation results (cases 1 and 2). Figure S2 shows the net change in ^{137}Cs inventory over the catchment between 1 January 2014 and 31 December 2015 from simulation case 2.

692 Table S1 Manning's roughness coefficient for each land use and vegetation

Land use and Vegetation	Manning's roughness coefficient ($m^{-1/3}$ s)
Japanese Cedar & Japanese Cypress	0.5
Larch plantation	0.5
Deciduous broadleaf	0.8
River	0.03

693 Table S2 Raindrop-induced erosion parameters

Land use and vegetation	Canopy height (m)	Stem storage (mm)	Crown covering (-)	Floor storage (mm)	Floor covering (-)
Japanese Cedar & Japanese Cypress	15	1.5	0.8	0.25	0.95
Larch plantation	15	1.5	0.8	0.25	0.95
Deciduous broadleaf	15	1	0.8	0.25	0.95
River	0	0	0	0	0

694 Table S3 Hydraulic parameters for grid-blocks in the surface soil layers

Soil	Land use	Subsurface	Intrinsic permeability (m/s)	Effective porosity (-)	Relative permeability curve and capillary curve
Forest brown soil	River	-	1×10^{-4}	0.7	Cohesive soil
	Forest	Weathered host rock	1×10^{-3}	0.5	Cohesive soil
		Deposit on slope surface	1×10^{-3}	0.5	Gravel soil
		River bed sand Gravel	1×10^{-3} (top 30 cm of surface soil)	0.5	Gravel soil
			1×10^{-4} (soil between 30-100 cm)	0.4	Sandy soil

695

696 Table S4 Hydraulic parameters for grid-blocks in the subsurface layers

Geology	Intrinsic permeability (m/s)	Effective porosity (-)
River bed sand gravel	1×10^{-4}	0.3
Deposits on slope surface	3×10^{-5}	0.3
Weathered host rock (west)	5×10^{-7} (horizontal) 1×10^{-8} (vertical)	0.2
Weathered host rock (east)	1×10^{-6} (horizontal) **1.5×10^{-7} (vertical)[a]**	0.2
Bedrock	1×10^{-8}	0.1

697 [a] Tuned for this study such that simulations matched measurements for peak water discharge

698 rates under storm flow conditions

699 Table S5 Sediment particle size distribution

Soil	Land use	Subsurface	Sediment representative particle size (mm)					
			0.001	0.01	0.1	0.3	1	5
Forest brown soil	River Forest	-	**0.01[a]**	**0.04[a]**	0.25	0.30	0.20	0.20
		Weathered host rock	**0.03[a]**	**0.42[a]**	0.15	0.2	0.1	0.1
		Deposit on slope surface	**0.03[a]**	**0.32[a]**	0.1	0.1	0.15	0.3
		River bed sand gravel	**0.03[a]**	**0.17[a]**	0.10	0.10	0.20	0.40

700 [a] Tuned for this study such that simulations matched measurements on suspended sediment

701 fluxes under base flow conditions

Table S6 Soil detachment properties

Soil	Land use	Subsurface	SDI (g/J)	Adhesion (kPa)
Forest brown soil	River	-	3.0	-
	Forest	Weathered host rock	**50**[a]	10
		Deposit on slope surface	**50**[a]	3
		River bed sand gravel	**50**[a]	3

[a] Tuned for this study such that simulations matched measurements for peak suspended sediment fluxes under storm flow conditions.

Table S7 Dissolved ^{137}Cs concentrations at the catchment outflow. Measurements taken subsequent to Tsuji et al. (2016).

Date	Dissolved ^{137}Cs concentration (Bq/L)
4 Aug. 2015	0.45
25 Aug. 2015	0.38
25 Sep. 2015	0.27
8 Oct. 2015	0.23
22 Oct. 2015	0.23
17 Nov. 2015	0.33
11 Dec. 2015	0.16

Table S8 Correlation between simulated and measured dissolved ^{137}Cs concentrations in river water at the catchment outflow under base flow conditions (n=33).

Simulation case	Percentage of results within a factor of 2 from measurements (%)	Pearson correlation coefficient, r
Case 1	79	0.13
Case 2	91	0.21

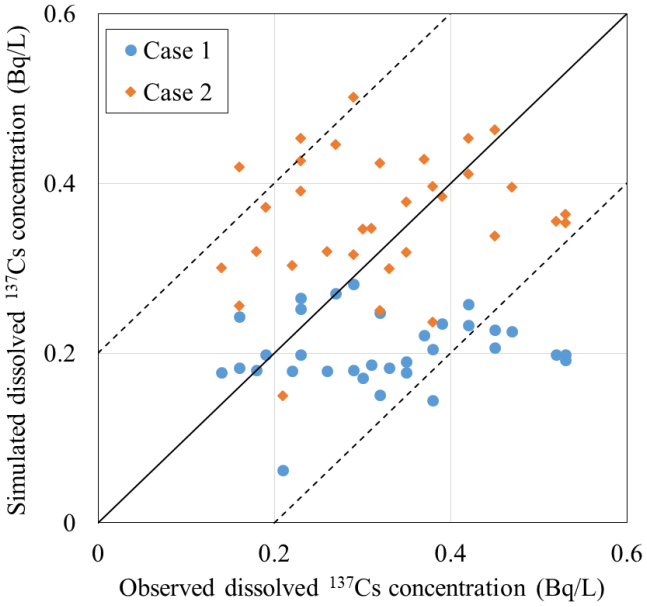

710

711 Figure S1 Scatter plot of dissolved ^{137}Cs concentrations at the catchment outlet under base
712 flow conditions (*n*=33), comparing measurements and simulations. Solid line indicates
713 equality, while dashed lines indicate bands within a factor of 2.

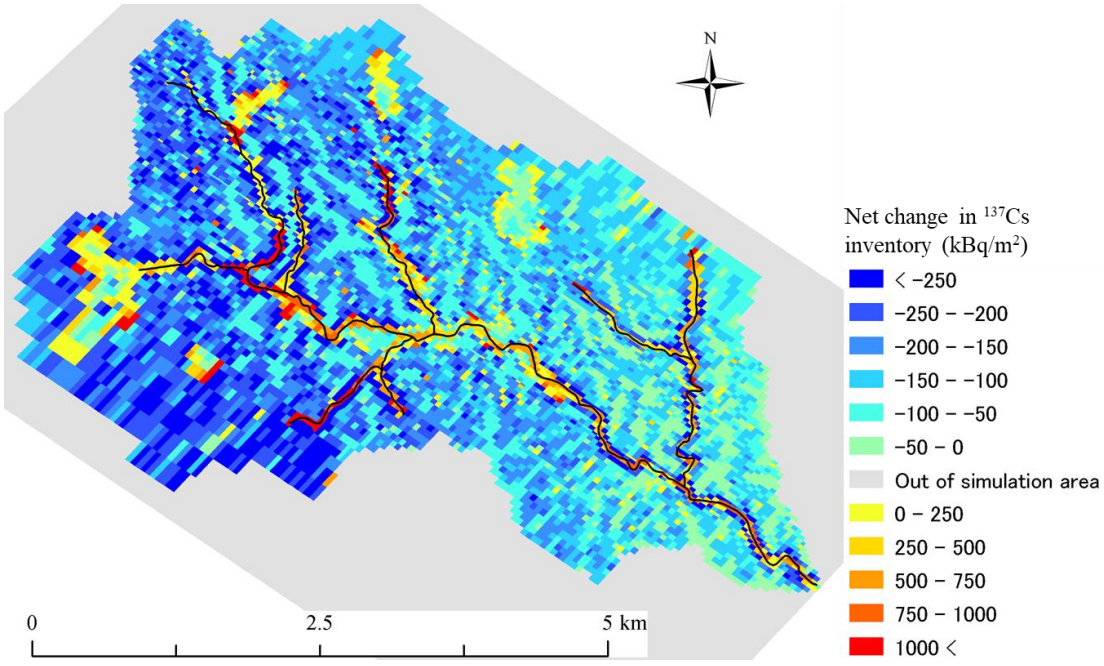

714

715 Figure S2 Case 2 simulation results for net change in ^{137}Cs inventory between 1 January 2014
716 and 31 December 2015.

References

Morgan, R.P.C., Quinton, J.N., Smith, R.E., Govers, G., Poesen, J.W.A., Auerswald, K., Chisci, G., Torri, D., Styczen, M.E., 1998. The European soil erosion model (EUROSEM): a dynamic approach for predicting sediment transport from fields and small catchments. Earth Surf. Process. Landf. 23, 27–544. doi:10.1002/(SICI)1096-9837(199806)

Sakuma, K., Kitamura, A., Malins, A., Kurikami, H., Machida, M., Mori, K., Tada, K., Kobayashi, T., Tawara, Y., Tosaka, H., 2017. Characteristics of radio-cesium transport and discharge between different basins near to the Fukushima Dai-ichi Nuclear Power Plant after heavy rainfall events. J. Environ. Radioact. 169-170, 130–150. doi:10.1016/j.jenvrad.2016.12.006

Sakuma, K., Malins, A., Funaki, H., Kurikami, H., Niizato, T., Nakanishi, T., Mori, K., Tada, K., Kobayashi, T., Kitamura, A., Hosomi, M., 2018. Evaluation of sediment and ^{137}Cs redistribution in the Oginosawa River catchment near the Fukushima Dai-ichi Nuclear Power Plant using integrated watershed modeling. J. Environ. Radioact. 182, 44-51. doi:10.1016/j.jenvrad.2017.11.021

Tsuji, H., Nishikiori, T., Yasutaka, T., Watanabe, M., Ito, S., Hayashi, S., 2016. Behavior of dissolved radiocesium in river water in a forested watershed in Fukushima Prefecture. J. Geophys. Res.: Biogeosciences 121, 2588-2599. doi:10.1002/2016JG003428